Paper: ASAT-16-112-PP

16th International Conference on
AEROSPACE SCIENCES & AVIATION TECHNOLOGY,
ASAT - 16 – May 26 - 28, 2015, E-Mail: asat@mtc.edu.eg
Military Technical College, Kobry Elkobbah, Cairo, Egypt
Tel : +(202) 24025292 – 24036138, Fax: +(202) 22621908

EXPERIMENTAL AND DESIGN CONSIDERATIONS FOR SOLID PROPELLANT GAS GENERATOR

Ah. El-S. Makled *

ABSTRACT

The main vital purpose of gas generator (GG) solid propellant (SP) is, the burning of SP to produce the required gas amount with low temperature and without solid precipitate. Numerous variety of propellants and configurations have been used to create hot gas.

A comprehensive study of several important aspects of SPGG design has been investigated in the present work. End burning mechanism, GG solid propellant types, various burning surface configurations, simplified design procedure, insulation evaluation, analysis of experimental works, numerical models have been developed to describe pressure variation with time and performance parameters. Effect of design parameters were also discussed.

Good agreement is obtained between experimental firing data and the established models for SPGG parameters performance. Finally; the several design parameters of the SPGG are analyzed and investigated, each design parameter is treated separately while the other parameters are assumed constant.

KEY WORDS

Solid propellant, gas generator, end burning

1: INTRODUCTION

GGs are classified according to propellant type, as liquid (bi-propellant and mono-propellant), solid and hybrid GG. Another classification is made according to the nozzle type as sub-critical and super critical GG [1,2].

The SPGG can be utilized for pumping and gas turbine driving, liquid propellant feeding system, moving actuators and mechanisms, separation units, airbags and hot air balloons inflation (deploy), electric power generation for missiles, thrust vector control, ……..etc.

The main characteristics of SPGG are fast operation, limited time of operation, high power generation, long time of storage (10-15 year), relatively small burning rate and simple design with small size.[3,4].

The principal elements of SPGG are shown in **Fig. (1)**, the igniter is used to start SP burning, filter to prevent or minimize the solid particles from the combustion gas and cooler system as heat sink material to minimize the combustion gas temperature.

Design objective for operational SPGG is the ability to produce gases safety, with required properties (temperature, pressure, non-explosive, harmless), in a compact unit at the required mass flow rate.

* Egyptian Armed Forces, Egypt.

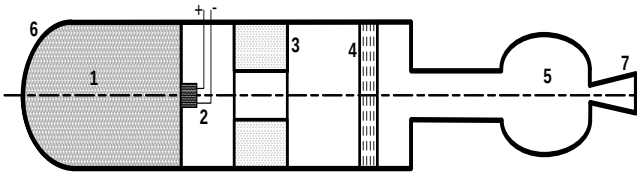

1- solid propellant 2- Igniter 3- cooler 4- Filter
5- Collector 6- Combustion chamber casing 7- Nozzle

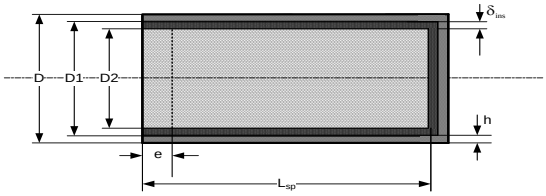

D is the outer diameter of the SPGG cch,
D1 is the inner diameter of the SPGG cch,
D2 is the SP grain outer diameter,
e is the increment burnt thickness,
Lsp is the SP grain length,
h is wall thickness of the SPGG cch.

Fig. (1) Principal scheme of SPGG

2: SOLID PROPELLANTS FOR GAS GENERATORS

The GGSP is based on the mixture of stabilized ammonium nitrate and different fuel binders with various shapes, to secure a required mass flow rates.

The GGSP requires creating clean combustion gas (smokeless and impurities) with low temperature (less than 1000 °C) and smooth burning rate (0.30÷12) mm/sec with long duration (up to 100 Sec) according to task, reliable and quick ignition, non-hazardous generated gas (in civil applications), long term storage (10-15 year), transporting and handling with low expense. Commonly, GGSP composition burned in fuel-rich mixture (O/F ≈0.5), to keep combustion temperature low. The GGSP can be divided into four groups based on the oxidizer type [1]:

1-Ammonium perchlorate NH_4C1O_4,
2-Ammonium nitrate NH_4NO_3,
3-Dihydroxylglyoxime $C_2H_4O_4N_2$ and
4-Nitramine $C_3H_6O_5N_6$ and $C_4H_8N_8O_8$ (Hexogen and octagon).

On the other side, the GGSP grain can be classified according to dimensions (web fraction W, length to diameter ratio (L/D) and volumetric loading fraction ή). **Table 1** describes different GGSP grain configurations characteristics [1,2,6].

Table (1).GGSP grain configuration [2,4,5]

Configuration	L/D ratio	ή	Burning mode	C.G Shift	W	Remarks
End side (rod)	> 1.0	0.90-0.95	Neutral	Large	> 1.0	Web thickness = grain length
Internal tube	< 2.0	0.85-0.95	Progressive	Small	0.5-1.0	Usually with unrestricted ends, 2<L/D<4 for slotted
Star	N.A	0.75-0.85	Combination	Small	0.3-0.6	Ideal for web fraction o.3 to 0.4 ;progressive above 0.4 , can be neutralized with slots
Wagon wheel	N.A	0.65-0.70	Combination	Small	0.2-0.3	wagon wheel common used 0.2

Most commonly used configuration is rod with high L/D, end burning face and protected by inhibitor material. The end-burning GGSP can be modified and controlled by initial convex burning surface to modified design performances. The SP grain configuration is known as "cigarette" burning with constant burning surface.

The inhibitor (restrictor) must be remained effective over burning period, satisfied mechanical and physical properties.

The SPGG insulator should fulfill these requirements:

1. It must be erosion resistant, that are chemically resistant to the hot gas and particulates.
2. It must provide good thermal resistance to limit heat transfer to the GG case and thus keep the case below its maximum allowable temperature.

3. It should be capable of transmitting stress and allow a large deformation or strain to accommodate grain deflection upon pressurization or temperature cycling.
4. Its decomposition temperature should be high.
5. It should have good adhesion or bonding qualities.
6. It should have a low density, thus reducing inert mass.

3: END BURNING MECHANISM

End burners typically are applicable to missions requiring relatively long durations and low thrust-levels.

The effect of heat transfer parameter on burning surface turns out to be significant; the non-regular burning surface will become visible.

As the burning time increased, the effect of heat transfer close to combustion chamber metal case enlarged as shown in **Fig. (2)**. The burning rate r_1 is the reference burning rate of the grain, r_2 is the burning rate at the propellant-metal interface, angle Θ is defined by the relative values of r_1 and r_2 and the instantaneous shape defined by the values of Δx and Δy.

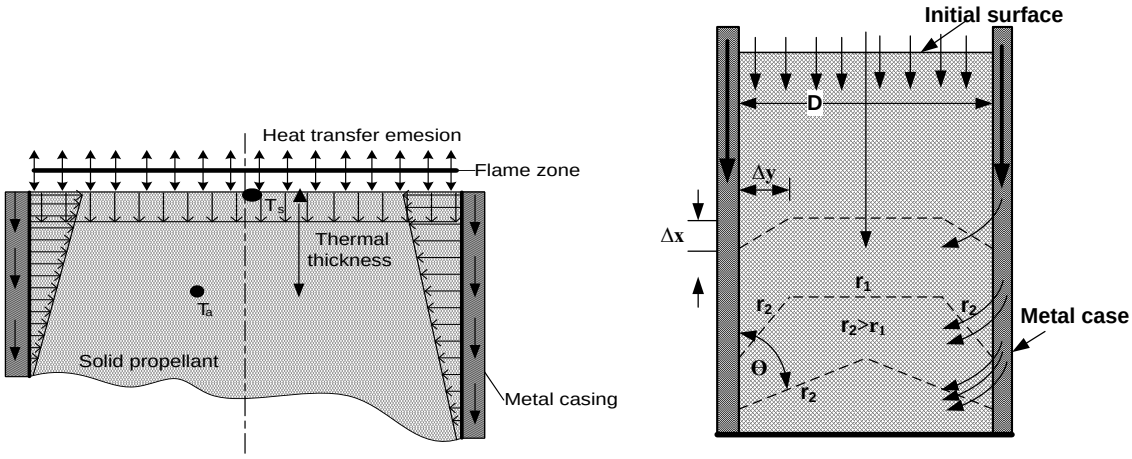

Fig. (2). End burning surface mechanism

The fundamental assumptions for the end burning surface combustion in GGSP are: [5]

1) The penetration depth of the temperature profile is small compared to the web thickness of the propellant charge,
2) The temperature gradient in the axial direction is small compared to the gradients in the normal direction,
3) Neglect the effect of all thermal stress by conduction as shown in **Fig. (2)**.

Under these conditions, the burning surface A_{bu} remains constant during burning and the burning rate is mainly function of the chamber pressure P_c and the equilibrium temperature at which the SP was soaked prior to ignition T_{sp}, the burning rate is described as [4]:

$$r = r_o . e^{kT(T_{sp} - T_N)} . P_c^n = aP_c^n \qquad \text{Eq. (1)}$$

Where, r ..linear burning rate of the propellant [m/s], r_o arbitrary constant burning rate at ambient temperature and atmospheric pressure [m/s], K_T temperature sensitivity of propellant [°C], T_{sp} temperature of propellant before burning [°C], T_N normal temperature [°C] and n burning rate pressure exponent.

4: SPGG CHARGE DESIGN

The chamber pressure is principally given by the relation of the A_{bu} to the nozzle throat area A_{th} (blocking factor K_I), in case of constant A_{th}, if the A_{bu} increases, the burning is so called progressive and vice versa digressive or neutral burning at $(A_{bu\,(t)} / A_{bu\,(i)}) \approx 1$

The form of the intial grain surface $A_{bu(i)}$ must be chosen in order to secure the required P_c or mass flow rate profile which is specified for definite mission (feeding system , moving turbine ,air bags , actuators ,…….etc)

In the cigarette burning, the filling coefficient K_{fc} is usually closed to one, (practicaly greater than 95%), the sliver ratio is less than 2% and the design grain length L_{sp} is:

$$L_{sp} = (1.01) r t_{bu} \qquad \text{Eq. (2)}$$

where the coefficient 1.01 takes into consideration possible losses of SP [4,5].
The mass of the SP charge m_{sp} can be written as:

$$m_{sp} = K_I A_{bu} L_{sp} \rho_{sp} \qquad \text{Eq. (3)}$$

The SPGG has to operate reliably within the temperature interval ($T_{min}\approx$-20ºC ÷ $T_{max}\approx$+50ºC). Then it is necessary that the P_c at T_{min} of SP charge will be stabile (coughing pressure), therefore the magnitude of the A_{th} has to be determined regarding the mentioned condition:

$$A_{th} = \frac{F_{\min}}{C_F P_c} = \frac{F_{\min} C^*}{I_{sp} P_{c\,\min}} \qquad \text{Eq. (4)}$$

Then the Eqs. (2, 3) can be reformed as:

$$m_{sp} = 1.01 \frac{F_{\min} t_{bu(\max)}}{I_{sp}} \qquad \text{Eq. (5)}$$

$$L_{sp} = 1.01 \frac{F_{\min} t_{bu(\max)}}{K_I A_{th} \rho_{sp} I_{sp}} \qquad \text{Eq. (6)}$$

where, $t_{bu(max)}$ is the operating time at T_{min} of SP charge, F thrust value, C_F thrust coefficient and SP qualifications parameters (ρ_{sp} SP density, C^* characteristic velocity, I_{sp} specific impulse).

4.1: GEOMETRIC ANALYSIS.

Special grain geometries that can be used with SPGG are shown in **Figs. (3, 4, 5)**, the shapes include convex, flat and compound end burning respectively. These geometries must satisfy the following points:

1) generate the required operating Pc and mass flow rate profile;
2) satisfy neutrality mode during firing time;
3) maximum filling coefficient, K_{fc}
4) small ratio of sliver;
5) minize the effect of heat transfer.

4-1-1: Convex Shape.

Fig. (3) describes SP convex shape with the basic dimensions [5], the burning surface can be written as:

$$A_{bu(i)} = A_{bu(A)} = A_{bu(B)} = 2\pi R_{(i)} X_{(i)} \qquad \text{Eq. (7)}$$

Where $R_{(i)}$ is the radius of the spherical shape, $X_{(i)}$ is the height of spherical segment.

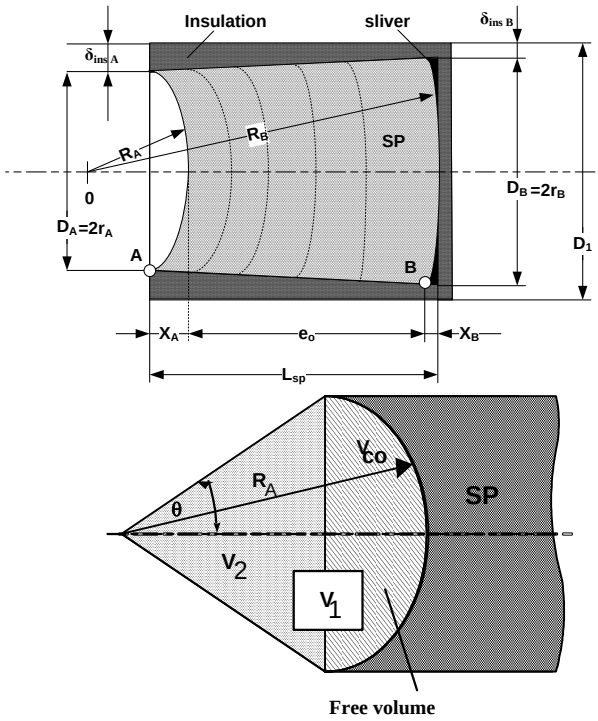

Fig. (3). convex shape for cegaret burning (front burning).

The basic parameters can be defined as the following:

The height of the spherical segment $$X_{(i)} = R_{(i)} - \left(R_{(i)}^2 - r_{(i)}^2\right)^{0.5} = \frac{A_{bu(i)}}{2\pi R_{(i)}} = \sqrt{\frac{A_{bu(i)} - \pi r_{(i)}^2}{\pi}}$$

The radius $r_{(i)}$ $$r_{(i)} = \frac{D_1 - 2\delta_{ins(i)}}{2} = \sqrt{\frac{A_{bu(i)} - \pi X_{(i)}^2}{\pi}} = \frac{1}{2\pi R_{(i)}}\sqrt{A_{bu(i)}\left(4\pi R_{(i)}^2 - A_{bu(i)}\right)}$$

The Initial radius of the spherical area R_A

$$R_A = R_B - e_O = \frac{A_{bu}}{2\pi\sqrt{\frac{A_{bu} - \pi\left(\frac{D_1 - 2\delta_{ins(B)}}{2}\right)^2}{\pi}}} - (1.01)aP_c^n t_{bu}$$

The design parameters can be defined as:

The thickness insulation at any point $$\delta_{ins(i)} = \frac{D_1 - D_{(i)}}{2}$$ Eq. (8-a)

The SP length $$L_{SP} = e_O + X_A = (1.01)aP_c^n t_{bu} + \frac{A_{bu}}{2\pi R_A}$$ Eq. (8-b)

The burning surface $A_{bu}(t) = 2\pi\left(R(t)\right)^2\left(1 - \cos\theta(t)\right)$ where $\theta = \sin^{-1}\frac{r_A}{R(t)}$ Eq. (8-c)

The filling coefficient, K_{fc} defined as

$$K_{fc(i)} = \frac{V_{SP}}{V_{cch}} = 1 - \frac{V_{co(i)}}{V_{cch}} = 1 - \left[\frac{8}{L_{sp}D_1^2}\left(\frac{1}{3}R_A^3\left[1 - \cos\theta_{(i)} - \frac{1}{2}\sin^2\theta_{(i)}\cos\theta_{(i)}\right]\right)\right]$$ Eq. (8-d)

Sliver ratio $$\eta_{sliver} = \frac{V_{sliver}}{V_{sp}} = \frac{V_{cyl} - V_{co(f)}}{V_{cch} - V_{co(A)}}$$ Eq. (8-e)

where

$$V_{co(i)} = \frac{2}{3}\pi R_A{}^3\left[1-\cos\theta_{(i)} - \frac{1}{2}\sin^2\theta_{(i)}\cos\theta_{(i)}\right]$$

$$V_{co(f)} = \frac{2}{3}\pi R_B{}^3\left[1-\cos\theta_{(f)} - \frac{1}{2}\sin^2\theta_{(f)}\cos\theta_{(f)}\right]$$

$$V_{cch} = \frac{\pi}{4}D_1^2 L_{sp}$$

The free volume is an equal volume of convex, V_{co} which is an equal volume of conical shape, V_1 remove volume of right cylindrical cone V_2 as $V_{fr(i)} = (V_{co(i)} - V_2) + V_{ig}$

The thickness of thermal stress protection in point "A" $\delta_{ins(A)}$ larger as in point "B" $\delta_{ins(B)}$ since the metal case near the nozzle effected for long time of burning

4-1-2: Flat Shape.

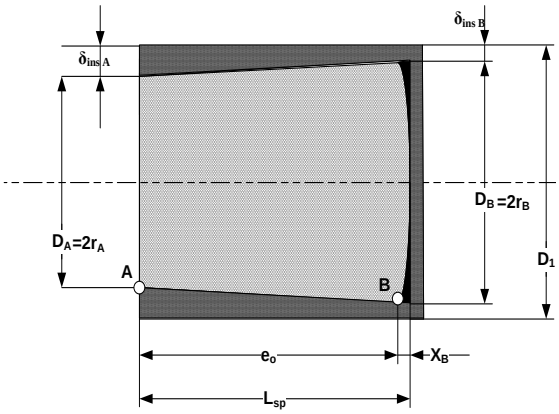

Fig. (4) Flat shape end burning.

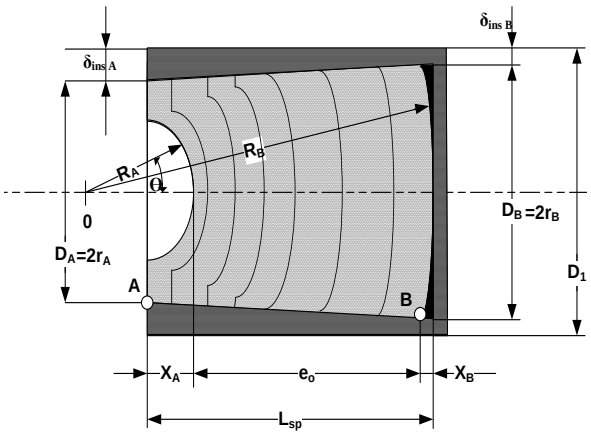

Fig. (5) Compound shape end burning.

Burring surface area: $A_{bu(i)} = \frac{\pi}{4}D_{(i)}{}^2$ Eq. (9-a)

Free volume $V_{fr} = V_{ig}$ Eq. (9-b)

Filling coefficient (K_{fc}) $K_{fc} = \frac{V_{SP}}{V_{cch}}$ Eq. (9-c)

Sliver rtaio $\eta_{sliver} = \frac{V_{sliver}}{V_{sp}} = \frac{V_{cyl} - V_{co(f)}}{V_{sp}}$ Eq. (9-d)

4-1-3: Compound Shape.

Burring surface area equal the annular flat area, A_{fl} in addition the convex area, A_{co}

$$A_{bu} = \frac{\pi}{4}\left[D_A{}^2 - \left(R(t)\sin\theta(t)\right)^2\right] + A_{co}$$ Eq. (10-a)

Free volume $V_{fr} = V_{co} + V_{ig} = \frac{2}{3}\pi R_A{}^3\left[1-\cos\theta - \frac{1}{2}\sin^2\theta\cos\theta\right] + V_{ig}$ Eq. (10-b)

Filling coefficient (K_{fc}) $K_{fc} = 1 - \frac{V_{co(i)}}{V_{cch}}$ Eq. (10-c)

Sliver ratio $\eta_{sliver} = \frac{V_{cyl} - V_{co(f)}}{V_{cch} - V_{co(i)}}$ Eq. (10-d)

Where:

$A_{co}(t) = 2\pi\left(R(t)\right)^2\left(1-\cos\theta(t)\right)$

$$V_{co} = \frac{2}{3}\pi R_A^{\,3}\left[1-\cos\theta-\frac{1}{2}\sin^2\theta\cos\theta\right]$$

5: EXPERIMENTAL WORK

The objectives of the experimental work could be summarized as follows:

1) Functioning test and evaluating performance of SPGG.
2) To evaluate the insulation efficiency.
3) To check the validity of the mathematical model.
4) To study the effect design parameters.

The early phase of study is to examine the suitable insulation material and suitable igniter for propellant charge from local market. Subsequent phases are the lab-test SPGGs design, manufacturing, inspection, cold testing, and preparion for firing tests as in **Table (2) and Fig. (6)**. The detail discussion about SPGG firing test and mathematical model validation are discussed in reference [6, 7].

After two successful achievement attempts to adjust the ignition, insulation, graphite nozzle and operating parameters, unfortunately third test is exploded as in **Fig. (7)** due to separation of insulation material form SP surface, that increases the area A_{bu} which in turns produces high P_c more than design value caused by explosion. The track of experimental is transformed to reach safety procession, The actual SPGG was used as shown in **Fig. (8).**

5-1: Insulator Evaluation

Double base propellant grain was machined under high safety precuations, to construct four SP charge for GG with length 50 mm and diameter 25 mm.

Four types of insulation materials are examined by coating SP charge with 1 mm thickness of each material as shown in the **Fig. (9)**.

1) RTV silicone high temperature (with stands 300°C).
2) Ratnge silicon (used with the small scale RM as coating material).
3) High temperature cement (inorganic cement), used for embedding heating elements and thermocouples (max service temp 1550 °C).
4) kevlar clothes (style 704).

The RTV silicon (1) and Ratnge silicon (2) was combustible during tests and left amount of reminders (ash) in the shape of black carbon particles. For previse reasons, these materials were excluded. Cement material (3) acting as excellent insulation and inhibitors during time of SP firing, but after firing it gets very brittle. Kevlar clothes (4) got red color and incombustible after test. Finally after investigation, Cement material was selected as an insulation and inhibitor material for SPGG.

5-1-1: Thermal Conductivity Evaluation

Fig. (10) describes the system of thermal conductivity evaluation for two standard specimens of Kevlar clothes and inorganic cement. The temperature differance between the steam chamber T1 and the brass slab T2 (measured by thermometers) and specimen dimensions (diameter, thickness), the current flow heat H1 at steady heat flow through the specimen is evaluated by:

$$H_1 = \frac{dQ}{dt} = KA\frac{(T_1 - T_2)}{dx} \qquad \text{Eq. (11)}$$

The result of tests get the thermal conductivity of Cement specimement ($k=8.18\times10^{-3}$ cal/s.cm.Co) higher than Fiber Carbon ($k=2.87\times10^{-3}$ cal/s.cm.Co).

5-2: Firing Tests and results

The SPGG design passed a series of cold tests (hydrostatic test) to minimize the risk of damage during firing **Fig. (6)**. Cold test has been accomplished using high pressure air (100 bar) for 15 minutes without any leakage or failures. The demonstration and function tests has been accomplished without any risk, unfortunately during third test.

Table (2). SPGG design characteristics

Parameter	Value
Wall thickness of cch, (mm)	2.25
Igniter mass, (g)	0.5
The length of the connected, (cm)	1.59
Molecular weight, (gm/mol)	22.64
Specific heat ratio	1.255
Characteristic velocity, (m/sec)	1403.0
Density of propellant, (kg/m^3)	1563
Temperature of combustion, (K)	2324
Nozzle throat diameter(mm)	2.5
mass flow rate range, (kg/sec)	0.117
operating ambient temperature,°C	20
operating pressure bar	50
design pressure, bar	91
operating time sec.	9.75

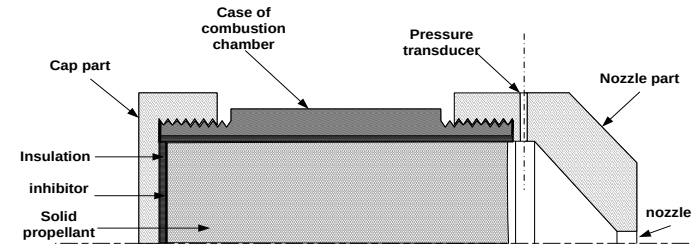

SPGG cch after firing graphite nozzle

Fig. (6). A simple designed of SPGG

Fig. (7). Residual parts after firing test number 3

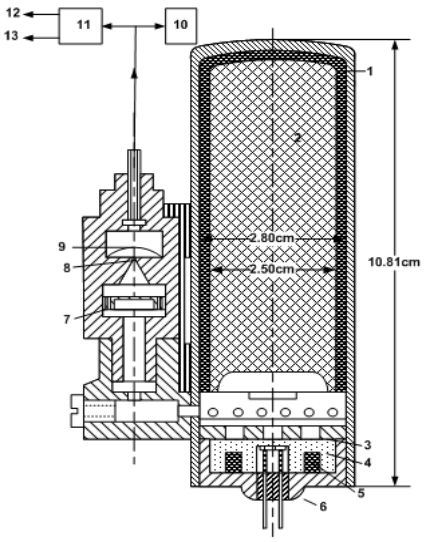

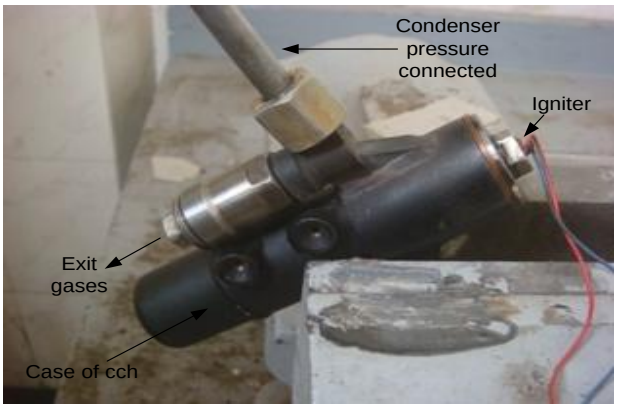

1-inhibitor, 2- propellant, 3- burst diaphragm,4- black powder, 5- combustion sustainer, 6- igniter assembly, 7-fuser, 8- nozzle, 9- filter, 10- control units, 11- electrical power generator, 12- guidance unit, 13-control unit.

Fig. (8) SPGG assembly for air defense missile

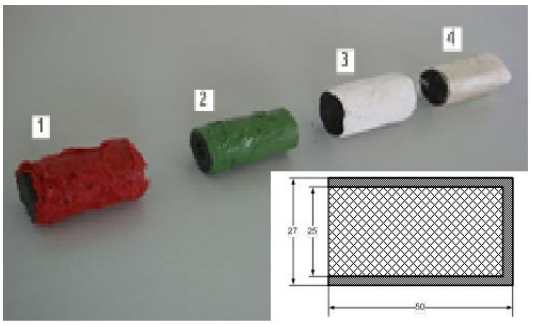

Fig. (9). SP charge with insulation materials

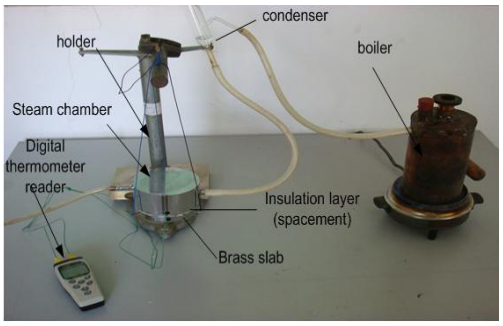

Fig. (10). Thermal conductivity measurments

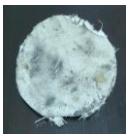

Kevlar clothes

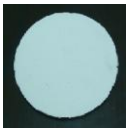

inorganic cement

Unexpexted explosion takes place, due to cement separation form SP charge, which causes increasing in burning surface and pressure over the safety valve operation (27 bar) as shown in **Fig. (7)**.

The real SPGG was used in firing tests as shown in **Fig. (8)**. The typical recorded pressure-time curves and performing data analysis at room temperature are shown in **Fig. (11)** and **Table (3).**

The SPGG propellant grain is extruded, the polymenthyl methacrylate inhibitor is cast in place and the grain is machined on one end to fit the dome of the SPGG chamber and on the igniter end to form the required end-burning surface [8].

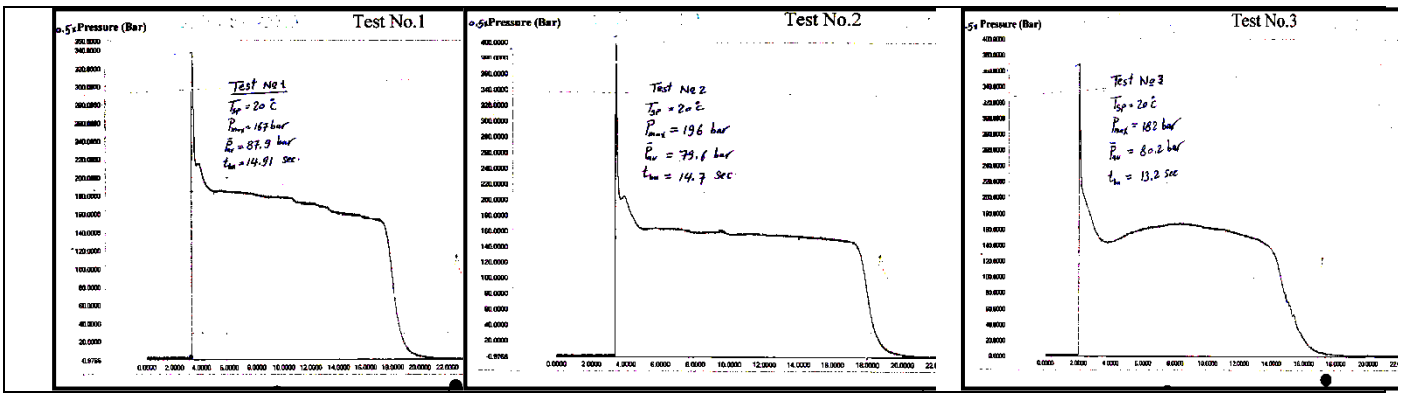

(test 1) (test 2) (test 3)

Fig. (11).Chamber pressure with time operation

Table (3). Experimental static firing results and evaluation

Parameter	Experimental				Theoritical			
	Test1	Test2	Test3	Average value	Program 1	Average error%	Program 2	Average error%
average pressure, $P_{c(av)}$ [bar]	87.90	79.6	80.20	82.57	85.31	3.3	81.20	1.7
Max. pressure, $P_{c(max)}$ [bar]	167	196	182	181.67	184.08	1.3	153.37	15
Burning time, T_{bu} [sec]	14.91	14.70	13.20	14.27	14.75	3.4	14.58	2.2
Average Burning rate, r_{av} [mm/sec]	6.03	6.12	6.81	6.32	6.10	3.3	6.17	2.2

The measured experimental data were compared with results obtained from theoretical computation. The comparison shows good agreement, as seen in **Table (3)**, which proves the validity of developed program, since the maximum error of the program is generally less than 4% except the value of maximum pressure the error reached 15% due to ignition phase assumptions.

6: DESIGN PARAMETERS INVESTIGATION

The effects of change in various design parameters are examined and the results compiled in the form of traces of chamber pressure versus operating time and tables. The model of air defence missile SPGG was used as a baseline for the current analysis. The effect of each design parameter is treated separately, i.e., other parameters are assumed constant. Different parameters are compared, for nearly the same filling coefficient. The investigated parameters include initial burning surface, SP initial temperature, SP grain length, nozzle critical diameter and pressure exponent (propellant ingredient).

6-1: Effects of SP Initial Temperature

The initial SP temperature affects the burning rate and hence the SPGG performance. The GGSP temperature sensitivity selected have a low temperature sensitivity of burning rate, particularly in those designs where the chamber pressure and generated gases level must be held within narrow margins over wide ranges of temperature. This parameter is investigated by adjusting the burning rate coefficient (a) according to Eq. (1).

The burning rate coefficient, which is based on an initial SP temperature (operating temperature -20 up to +50°C) and T_N is the normal temperature equal 20°C.

The results are shown in **Fig. (12)** for various initial grain temperatures.

It is noted that, the chamber pressure increases as the initial SP temperature increases. Moreover, it is found that burning time reduces as the initial SP temperature increases.

Generally, the following remarks can be drawn from the analysis of the shown results.

- The change of average pressure is within 77% while the operating time varies in the range of 72% and average burning rate about 77%
- As the initial grain temperature increases the burning rate and (consequently) the average and maximum chamber pressures increase while the T_{bu} decreases.
- The temperature change has approximately the same of the total impulse.

Table (4) The result for various initial grain temps

Parameter	initial SP temperature		
	-10°C	**20°C (Base line)**	50°C
average pressure, P_{av} [bar]	58.24	**85.31**	124.99
average pressure, $P_{c(av)}$ [bar]	125.66	**184.08**	269.69
Max. pressure, $P_{c(max)}$ [bar]	21.25	**14.75**	10.34
Burning time, T_{bu} [sec]	4.15	**6.09**	8.91

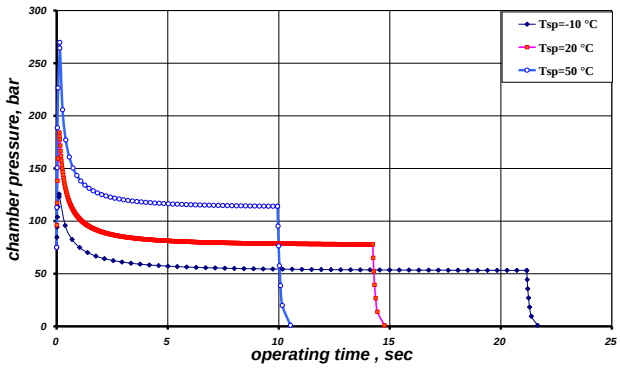

Fig. (12). Chamber pressure versus time for various initial grain temperature

6-2: Effects of Initial Burning Surface

The effect of changing the initial burning surface on the pressure time curve is analyzed and compared to the flat end burning. The average pressure and operating time of SPGG during pseudo equilibrium operation are kept approximately the same as shown in **Fig. (11)**. The initial burning surface is investigated by arbitrary variation of the convex angle θ_o, of the initial burning surface as derived in the following equations.

$$\theta_o = \sin^{-1}\frac{D_2}{2(y_o + e)} \qquad \text{Eq. (12)}$$

$$A_{bu} = 2\pi(y_o + e)^2.\left[1 - \cos\left[\sin^{-1}\frac{D_2}{2(y_o + e)}\right]\right] \qquad \text{Eq. (12)}$$

Computations were made for these values

- approximate by flat burning surface $\theta_o \approx 20°$

- approximate by hemi sphere burning surface $\theta_o \approx 60°$(based line)
- approximate by convex shape burning surface $\theta_o \approx 85°$

The results are shown in **Fig. (14)** and **Table (5)** along with the base line results. The maximum pressure strongly affected by the initial shape of the burning surface. It is found that 10% of operating chamber pressure will change with a low variation of burning time and burning rate.

6-3: Effects of SP Grain Length, L_{sp}

The choice of the GGSP grain length according to operating time mission, since SP burning rate depends on web thickness. The effect of end burning SP grain length at constant filling coefficient are shown on **Fig. (15)** and **Table (6)**. For the final operating times have shown large variation with constant operating pressure due to change of web thickness.

Table (5). Result for various initial burning surface configurations

Parameter	initial burning surface configuration(Θo(deg))			
	θ_o =20° ≈ flat surface	θ_o =40°	θ_o **=60°** **(Base line)**	θ_o =85° ≈ hemi sphere surface
average pressure, $P_{c(av)}$ [bar]	78.50	81.97	**85.31**	89.48
Max. pressure, $P_{c(max)}$ [bar]	84.47	112.24	**184.08**	488.30
Burning time, T_{bu} [sec]	15.23	14.97	**14.75**	14.63
Average Burning rate, r_{av} [mm/sec]	6.07	6.08	**6.09**	6.08

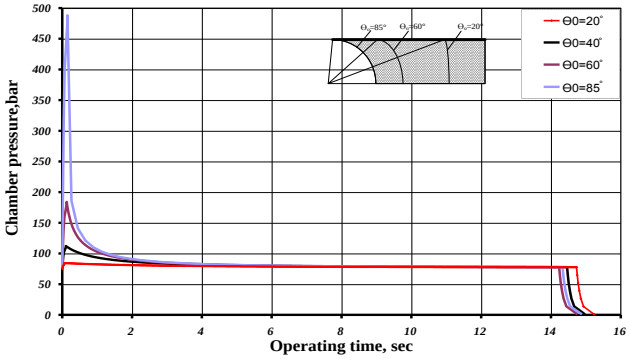

Fig. (14). Chamber pressure versus time for various initial burning surface configuration

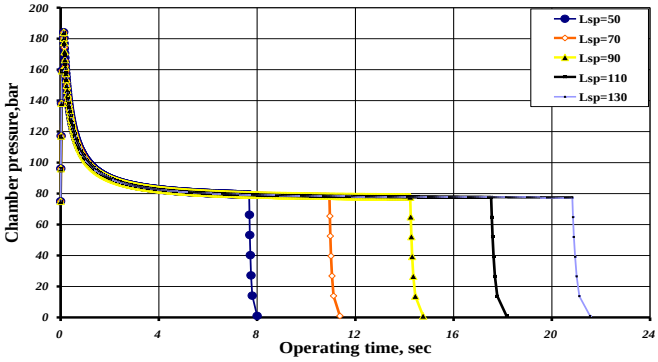

Fig. (16). Chamber pressure versus time for various SP grain lengths

Table (7). Result for various SP grain lengths

Parameter	SP grain length (mm)				
	50.0	70.0	**90.0** **(Base line)**	110.0	130.0
average pressure, $P_{c(av)}$ [bar]	90.82	87.19	**85.31**	83.95	82.89
Max. pressure, $P_{c(max)}$ [bar]	184.14	184.10	**184.08**	184.08	184.08
Burning time, T_{bu} [sec]	8.00	11.37	**14.75**	18.15	21.55
Average Burning rate, r_{av} [mm/sec]	6.16	6.11	**6.09**	6.07	6.06

6-4: Effects of Nozzle Critical Diameter

Fig. (16) and **Table (7)** shows the effect of the critical exhaust diameter on the chamber pressure at various times. It can be seen that, the effect is along phase of trace P-t curve and SPGG performance. The higher critical diameter producing significant lower chamber pressure, as the burning progresses.

6-5: Pressure Exponent (Combustion Index)

In most operating solid propellants, the values for the pressure exponent of burning rate n, ranges from a low of 0.3 to a high of 0.8 [6]. The effect of n on the SPGG performance is shown in **Fig. (18)** and **Table (9)**, according to the following relation.

$$P_c \; \alpha \left(\frac{A_{bu}}{A_{cr}} \right)^{\frac{1}{1-n}}$$

From the above relation, as n increases, the effect of (A_{bu}/A_{cr}) on P_c becomes more important and essential. If n is large, an increase in A_{bu} will result again as possible so that the SPGG internal ballistics will not change significantly

Table (8). Result for various critical diameters

Parameter	critical diameter (mm)		
	0.80	**1.00 (Base line)**	1.20
average pressure, $P_{c(av)}$ [bar]	330.08	**85.31**	28.25
Max. pressure, $P_{c(max)}$ [bar]	711.98	**184.08**	75.00
Burning time, T_{bu} [sec]	7.01	**14.75**	30.07
Average Burning rate, r_{av} [mm/sec]	15.07	**6.09**	2.90

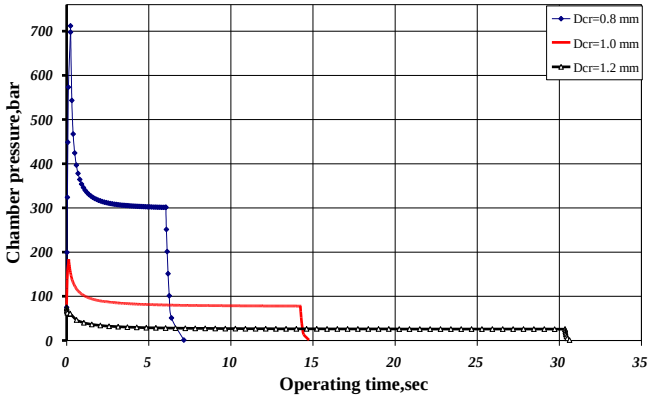

Fig. (17). Chamber pressure versus time for various critical diameters

Table (9). Result for various pressure exponents

Parameter	**Pressure exponent**		
	0.66	**0.67 (Base line)**	0.68
average pressure, $P_{c(av)}$ [bar]	53.33	**85.31**	140.57
Max. pressure, $P_{c(max)}$ [bar]	112.55	**184.08**	310.52
Burning time, T_{bu} [sec]	23.11	**14.75**	9.30
Average Burning rate, r_{av} [mm/sec]	3.82	**6.09**	9.99

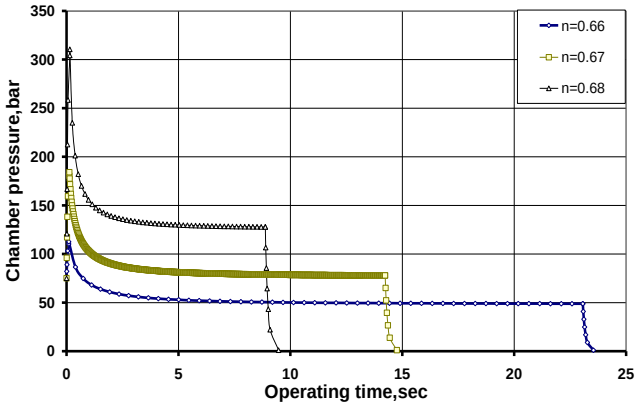

Fig. (18). Chamber pressure versus time for various pressure exponents

7: CONCLUSIONS

End burning GGSP mechanism has been investigated due to increasing of thermal stresses on metal casing of the combustion chamber. The evaluation of insulation material due to measuring of thermal conductivity and visual inspection after tests have been discussed and performed, the fiber carbon supported by cement material can be used as an insulation for SP charge from thermal conductivity and uncombustable points of view.

Problems related to SPGG design parameters, grain configuration, insulations and insulation have been discussed.

SPGG end buring with different intial buring surface program has been implemented and applied for the calculation of the pressure-time history and performance parameters.

Checking the validity of the proposed mathematical model and the computational solution is done through the comparison of computational and experimental results.

Comparison of computational and experimental results showed reasonable agreement with a maximum of 4% error. The program is considered as an effective tool for the evaluation of the SPGG end buring grain.
The SPGG design parameters have been investigated based on the mathematical program, to reduces the number of experiments needed to investigate the effects of varying geometrical or operational conditions of the SP grain.

6. REFERENCES

[1] Alain Davenas , “Solid Rocket Propulsion Technology”, Paris 1988.
[2] Barrere, M., ‘Rocket Propulsion’ Elsevier publishing company, 1960.
[3] D.K. Huzel and David .H. Huang, “Modern Engineering For Design of Liquid-Propellant Rocket Engines", Washington, Dc 20024,ISBN 1-56347-013-6,AIAA, 1992.
[4] Sutton, G., ‘Rocket Propulsion Elements’. Sixth Edition, John Wiley &Sons, New York, 1992.
[5] Ludvik, F., “Design and Manufacturing of Rocket Solid Propellant” short course, printed Lectures, Brno, 2001.
[6] Ah. Makled and W. B.El-hasumi “Modeling of End-Burning Solid Propellant Gas Generator” 75-PP, ASAT-15, MTC, Cairo, May 2012.
[7] Wesam El-hasumi “Theoretical and Experimental Investigation of Solid Propellant Gas Generator” MSc thesis, MTC, Cairo, Egypt, Aug. 2009.
[8] user’s manual ”SAM-7 air defense missile” confidential document.